FBP reconstruction of cone-beam data acquired with a vertex path containing a circle

Frédéric Noo, Michel Defrise, Rolf Clack
University of Liège (Belgium), Free University of Brussels (Belgium), University of Utah (U.S.A.)

Abstract

The paper presents a reconstruction algorithm for cone-beam (CB) data acquired with a vertex path which consists of a circle and of a complementary path such that Tuy's data sufficiency condition is fulfilled. The algorithm is based on the CB filtered-backprojection method of Defrise and Clack, with an appropriate handling of redundancy to reduce the processing of the circle data to a stationary 2D filtering. The method is similar to a previous algorithm of Kudo and Saito, and it also admits reconstruction from truncated data. However, the use of a 2D filter for the circle data instead of a 1D ramp filter avoids singularities in the filtered projections.

I. Introduction

The problem of cone-beam tomography consists of reconstructing a 3D image from cone-beam (CB) projections sampled along a specified trajectory called the vertex path.

The simplest vertex path consists of a circle about the object. Circle data can be efficiently reconstructed using the filtered backprojection algorithm (FDK) of Feldkamp et al [1], but the result is approximate. Stable and accurate reconstruction is possible only for complete paths: those which satisfy Tuy's condition [2]. Invoking Grangeat's [3] and Smith's results [4], Defrise and Clack [5], and independently Kudo and Saito [6], derived in 1994 a filtered backprojection (FBP) algorithm which yields exact reconstruction when CB data are measured along a complete vertex path. Unfortunately, the filtering step for these exact algorithms is nonstationary, and the FDK algorithm remains more attractive from the point of view of numerical efficiency.

This observation suggests combining the efficiency of the FDK algorithm with the analytic accuracy of fully 3D FBP algorithms. This combination is possible for "circle-plus" vertex paths which consist of a circle plus a supplementary curve designed to ensure that Tuy's condition is satisfied. The circle data can be reconstructed using the FDK algorithm, while the rest of the CB projections are reconstructed using the exact FBP algorithm [5] [6]. This composite algorithm has been investigated by Kudo and Saito [7]. Their remarkable work also showed the ability of the composite algorithm to handle truncated data.

This paper presents a rigourous analysis of the CB reconstruction problem for arbitrary circle-plus vertex paths. The exact DC-FBP algorithm of Defrise and Clack [5] is reviewed in section 2. The interplay between data redundancy and nonstationarity of the filtering step is investigated in section 3. In section 4 circle-plus vertex paths are considered and the composite algorithm is derived. A major result of this derivation is that some filtered projections contain singularities, which are illustrated in section 4.B for the particular case of a circle-plus-one-line path. A new composite algorithm is proposed in section 4.C, which avoids the singularities, processes the circle data as efficiently as FDK, and yields accurate reconstruction from truncated data. Results from simulated data are presented in section 5 to illustrate the accuracy and efficiency of the new algorithm.

II. FBP reconstruction of CB data

A. DC-FBP algorithm

We consider the problem of reconstructing an object from CB projections sampled along a complete vertex path about the object. The vertex path is parameterized by a scalar λ varying in some interval Λ of $\mathbb{R}$, and the vertex point is denoted by $a(\lambda)$. The object is represented by a smooth function $f(x)$ of finite support Ω (throughout the paper continuously differentiable functions are called smooth functions). The CB projections

$$g(u,v,\lambda) = \int_0^\infty dt\, f(a(\lambda) + t\beta(u,v,\lambda)) \qquad (1)$$

are collected on a 2D detector described using cartesian coordinates (u,v). Each line integral $g(u,v,\lambda)$ corresponds to a line of direction $\beta(u,v,\lambda)$ connecting the vertex point to some point (u,v) on the detector. The distance between the vertex point and the detector is denoted by D. Unless specified, we assume that the CB projections are not truncated.

The DC-FBP algorithm is a FBP method which, subject to some conditions discussed below, yields exact reconstruction. Mathematically, the algorithm applies to piecewise smooth vertex paths, for which the tangent vector $a'(\lambda)$ exists almost everywhere.

The reconstruction algorithm consists of performing a scaling and nonstationary filtering of the CB projections, followed by a 3D backprojection:

0-7803-3534-1/97 10.00©1997IEEE

Step 1 The CB projections are scaled

$$g_S(u,v,\lambda) = \frac{D}{\sqrt{u^2+v^2+D^2}}\, g(u,v,\lambda) \qquad (2)$$

Step 2 A nonstationary filter is applied. The filtered projections $g_F(u,v,\lambda)$ are equal to the 2D backprojection:

$$g_F(u,v,\lambda) = \int_0^\pi d\mu\, k_F(u\cos\mu + v\sin\mu, \mu, \lambda) \qquad (3)$$

of the filtered sinogram function

$$k_F(s,\mu,\lambda) = -\frac{1}{4\pi^2}\frac{\partial}{\partial s}\left\{\frac{\sqrt{s^2+D^2}}{D^2} M(s,\mu,\lambda)\right.$$
$$\left. |a'(\lambda)\cdot\theta(s,\mu,\lambda)|\,\frac{\partial}{\partial s}(\mathcal{R}g_S)(s,\mu,\lambda)\right\} \qquad (4)$$

defined on the λ-detector. The sinogram variables (s,μ) define a straight line $\mathcal{L}(s,\mu)$ in the detector plane and $(\mathcal{R}g_S)(s,\mu,\lambda)$ is the integral of $g_S(u,v,\lambda)$ along this line. The explanation of the weighting factor $|a'(\lambda)\cdot\theta(s,\mu,\lambda)|\, M(s,\mu,\lambda)$ is given below.

Step 3 The filtered CB projections are backprojected in 3D to form the reconstructed image

$$f_R(x) = \int_\Lambda d\lambda \frac{u^2+v^2+D^2}{||x-a(\lambda)||^2}\, g_F(u,v,\lambda) \qquad (5)$$

where, for λ fixed, (u,v) is the intersection of the detector with the line connecting x to the vertex point.

The significance of the factor $M(s,\mu,\lambda)\,|a'(\lambda)\cdot\theta(s,\mu,\lambda)|$ at some point (s_0,μ_0,λ_0) is the following. The vector $\theta(s_0,\mu_0,\lambda_0)$ has unit length, and is normal to the plane Π containing the line $\mathcal{L}(s_0,\mu_0)$ and the point $a(\lambda_0)$. The value $M(s_0,\mu_0,\lambda_0)$ is the relative weight given to the plane Π to account for its multiple intersections with the vertex path. The plane Π intersects the vertex path at $n(\Pi)$ vertices $a(\lambda_\alpha)$, $\alpha = 0,\ldots,n(\Pi)-1$ with lines $\mathcal{L}(s_\alpha,\mu_\alpha)$ on associated λ_α-detectors. In the absence of noise, data corresponding to each $(s_\alpha,\mu_\alpha,\lambda_\alpha)$ triple supply identical contributions to the image and must be given a relative weight $M(s_\alpha,\mu_\alpha,\lambda_\alpha)$ so that the total contribution is unity:

$$\sum_{\alpha=0}^{n(\Pi)-1} M(s_\alpha,\mu_\alpha,\lambda_\alpha) = 1 \qquad (6)$$

This relation is called "normalisation condition" and must be satisfied for each triple (s_0,μ_0,λ_0) associated with any plane Π intersecting the support Ω of $f(x)$.

The easiest way to satisfy the normalisation condition (6) is to take $M(s_\alpha,\mu_\alpha,\lambda_\alpha) = 1/n(\Pi)$. This choice is inappropriate because the M function would be discontinuous and the outer derivative in equation (4) would be numerically unstable.

The DC-FBP algorithm is a stable and exact method for solving the CB reconstruction problem provided the vertex path is complete and a smooth M function satisfying the normalisation condition (6) can be defined. A suitable expression for M was given in [5].

B. FDK algorithm

The FDK algorithm [1] is designed for approximately reconstructing CB projections sampled along a circle. The λ-detector is perpendicular to the plane of the circle and parallel to the vector $a'(\lambda)$. The u-axis is oriented along $a'(\lambda)$. The FDK and DC-FBP algorithms are similar except for the filtering step which for FDK reduces to

$$g_F(u,v,\lambda) = \int_{-\infty}^{+\infty} du'\, r(u-u')\, g_S(u',v,\lambda) \qquad (7)$$

where $r(u)$ is the kernel of the 1D ramp filter.

III. Redundancy handling

A. From nonstationary to stationary filtering

The filtering step in DC-FBP, equations (3) and (4), is the combination of simple 2D operations some of which can be efficiently implemented using linogram techniques [8]. Nevertheless, the succession of projection, differentiations and backprojection is more complex than the 1D ramp filtering in FDK, equation (7). This complexity increases the reconstruction time and the interpolation errors due to discretization. We have found [9] that, given a particular orientation of the detector, certain choices of the M function reduce the nonstationary filtering to a 2D stationary filtering, which can be efficiently implemented using 2D FFT code.

Assume that for a given $\lambda \in \Lambda$, the tangent vector $a'(\lambda)$ is parallel to the detector and is oriented along the u-axis. If $M(s,\mu,\lambda)$ is independent of s, i.e. $M(s,\mu,\lambda) = \overline{M}(\mu,\lambda)$, then the 2D Fourier transforms of g_F and g_S are linked by a simple 2D filter

$$\mathcal{F}_2 g_F(k_u,k_v,\lambda) = H_\lambda(k_u,k_v)\,\mathcal{F}_2 g_S(k_u,k_v,\lambda) \qquad (8)$$

the expression of which is given by

$$H_\lambda(k_u,k_v) = \frac{1}{D}\,|k_u|\,\overline{M}(\arctan\frac{k_v}{k_u},\lambda) \qquad (9)$$

where the arctan function is defined with its value in $[0,\pi)$. Note that equation (9) reduces to the 1D ramp filter when $\overline{M}$ is constant. More details can be found in [9].

Thus, if we can find solutions $M(s,\mu,\lambda)$ to the normalisation condition which for some λ are independent of s, then for those values of λ, faster and more accurate filtering will be possible. The composite algorithms in section IV are based on this idea.

B. Support of the kernel

Another disadvantage of DC-FBP is the global action of the filter. Owing to the projection and backprojection

steps in equations (3) and (4), the value of the filtered projection $g_F(u,v,\lambda)$ at any point (u_0,v_0) depends on the value of the projection data $g(u,v,\lambda)$ at all u and v. In contrast, in FDK, the value $g_F(u_0,v_0,\lambda)$ depends only on the projection data $g(u,v,\lambda)$ along the line $v=v_0$ parallel to the u-axis in the detector plane.

We have investigated the kernel support of the 2D stationary filter of equation (9) and found that its action is that of a ramp filter in the u-direction plus a weighted sum of ramp filtering in a range of directions inclined at an angle α with respect to the u-axis. Specifically,

$$g_F(u,v,\lambda) = \frac{\overline{M}(\frac{\pi}{2},\lambda)}{D}\, g_R^0(u,v,\lambda) + \int_0^\pi d\alpha\, q(\alpha)\, g_R^\alpha(u,v,\lambda) \tag{10}$$

where $g_R^\alpha(u,v,\lambda)$ is the result of the convolution of $g_S(u,v,\lambda)$ with the ramp kernel along the direction making an angle α with the u-axis:

$$g_R^\alpha(u,v,\lambda) = \int_{-\infty}^{+\infty} du'\, r(u') g_S(u-u'\cos\alpha, v-u'\sin\alpha, \lambda) \tag{11}$$

The function $q(\alpha)$ is given by

$$q(\alpha-\frac{\pi}{2}) = \frac{\sin\alpha}{D}\,\overline{M}'(\alpha,\lambda) - \frac{\cos\alpha}{2D}\,\overline{M}''(\alpha,\lambda) \tag{12}$$

where $\overline{M}'$ and $\overline{M}''$ are the first and second derivative of $\overline{M}(\mu,\lambda)$ w.r.t. μ, and $\overline{M}(\mu+\pi,\lambda)=\overline{M}(\mu,\lambda)$.

If for some small $\mu_0 \in [0,\pi/2]$, $\overline{M}(\mu,\lambda)$ is constant in the range $\mu \in [\pi/2+\mu_0, 3\pi/2-\mu_0]$ then the function $q(\alpha)$ in (10) is only nonzero on the range $[0,\mu_0]\bigcup[\pi-\mu_0,\pi]$ and the filter kernel has a wedge-shaped support of aperture $2\mu_0$ about the u-axis.

IV. Composite algorithms

A. The composite algorithm

The vertex path $a(\Lambda)$ considered in this section is the union of two subpaths $a(\Lambda_1)$ and $a(\Lambda_2)$ with $\Lambda=\Lambda_1\bigcup\Lambda_2$. The subpath $a(\Lambda_1)$ is a circle in the plane $z=0$. The λ-detector is oriented so that u- and v-axes can be chosen along $a'(\lambda)$ and the z-axis. The subpath $a(\Lambda_2)$ consists of one or more segments of curves such that the circle-plus path $a(\Lambda)$ is complete.

The application of DC-FBP with the smooth M function of [5] generally involves a nonstationary filtering of each CB projection, which is rather complex numerically. A more efficient approach for a "circle-plus" path consists of processing the circle data using FDK, and appropriately processing the rest of the data to achieve an exact reconstruction. This method is referred to as the composite algorithm. Applying FDK to the circle data is equivalent to applying DC-FBP with $M(s,\mu,\lambda\in\Lambda_1)=1/2$ (see [5]). The normalisation condition (6) can then be fulfilled only by taking the following expression for $M(s,\mu,\lambda\in\Lambda_2)$:

$$M(s,\mu,\lambda\in\Lambda_2) = \begin{cases} M_C(s,\mu,\lambda) & \text{if } \Pi(s,\mu,\lambda)\bigcap a(\Lambda_1)=\emptyset \\ 0 & \text{otherwise} \end{cases} \tag{13}$$

where $\Pi(s,\mu,\lambda)$ is the plane defined by the triple (s,μ,λ), and $M_C(s,\mu,\lambda)$ must satisfy a normalisation condition similar to (6), but restricted to those planes intersecting the subpath $a(\Lambda_2)$ but not intersecting the circle. A suitable expression for $M_C(s,\mu,\lambda)$ can be obtained by applying the general formula of [5] to $a(\Lambda_2)$. The filtered projections are then obtained:

- using equation (7) for the circle data, $\lambda\in\Lambda_1$
- using equations (3) and (4) for $\lambda\in\Lambda_2$, with the M function in (13)

Note that although the normalisation condition is satisfied, smoothness is not assured; this aspect is discussed below.

B. Singularities in the composite algorithm

To simplify the discussion, we restrict to the case where $a(\Lambda_2)$ is a line segment orthogonal to the circle through some circle point. The detector is parallel to the line and perpendicular to the circle, with the v-axis parallel to the z-axis. The M function in (13) then becomes:

$$M(s,\mu,\lambda\in\Lambda_2) = \begin{cases} 1 & \text{if } \Pi(s,\mu,\lambda)\bigcap a(\Lambda_1)=\emptyset \\ 0 & \text{otherwise} \end{cases} \tag{14}$$

Given a fixed μ, $M(s,\mu,\lambda\in\Lambda_2)$ is discontinuous in s at the point $s_c(\mu)$ where the plane $\Pi(s,\mu,\lambda)$ is tangent to the circle. This discontinuity results in singularities in the filtered projection $g_F(u,v,\lambda)$ along the curve $\mathcal{C}$ which is the CB projection of the circle. The general proof of this result is beyond the scope of this paper, but the argument can be sketched as follows. Owing to the action of the outer s derivative in (4) on the discontinuity of M, the function $k_F(s,\mu,\lambda)$ contains a boundary term proportional to $\delta(s_c(\mu)-s)$. The corresponding contribution of this boundary term to the filtered projection is

$$\int_0^\pi d\mu\,[\ldots]\,\delta(s_c(\mu)-u\cos\mu-v\sin\mu) = \sum\nolimits_i [\ldots]/|\frac{ds_c}{d\mu}(\mu_i^*)+u\sin\mu_i^*-v\cos\mu_i^*| \tag{15}$$

where μ_i^* are the angles, if any, such that $u\cos\mu_i^* + v\sin\mu_i^* = s_c(\mu_i^*)$. A simple geometrical argument shows that the expression in (15) is singular for any point (u,v) lying on $\mathcal{C}$. It can be shown that this singularity also occurs if the μ integral and the outer s derivative in equations (3) and (4) are permuted as in the algorithm of Kudo and Saito [6].

C. New composite algorithm

We derive in this section a new composite algorithm which avoids singularities and reconstructs the circle data

using a 2D stationary filtering which can be implemented almost as efficiently as the 1D ramp filter in FDK.

The singularities in the composite algorithm arose from the discontinuity of M for the planes $\Pi(s_c(\mu), \mu, \lambda \in \Lambda_2)$ which are tangent to the circle. Hence, to avoid this discontinuity, it is necessary to replace the weight function used for the circle data in the composite algorithm, $M(s, \mu, \lambda \in \Lambda_1) = 1/2$, by another function which smoothly tends to zero as the plane $\Pi(s, \mu, \lambda \in \lambda_1)$ tends to be tangent to the circle, that is, as μ tends to $\pi/2$. On the other hand, to satisfy the normalisation condition, the weight $M(s, \mu, \lambda \in \Lambda_1)$ should be equal to $1/2$ for all planes which do not intersect $a(\Lambda_2)$. A smooth expression for $M(s, \mu, \lambda \in \Lambda_1)$ which meets these constraints is:

$$\overline{M}(\mu, \lambda \in \Lambda_1) = \begin{cases} \frac{1}{2} & \text{if } |\cos\mu| > \sin\mu_0 \\ \frac{1}{2}\left(1 - \exp\left(\frac{\cos^2\mu}{\cos^2\mu - \sin^2\mu_0}\right)\right) & \text{otherwise} \end{cases} \quad (16)$$

where μ_0 is a small fixed angle. Note that this function is independent of s and hence, according to the results in section 3.B, the filtering of the circle data will be stationary. Given equation (16) for the circle data, it can be shown that the normalisation condition for the composite path $a(\Lambda_1) \bigcup a(\Lambda_2)$ is satisfied by the following choice of M for the subpath $a(\Lambda_2)$:

$$M(s, \mu, \lambda) = \begin{cases} M_C(s, \mu, \lambda) & \text{if } \Pi(s, \mu, \lambda) \bigcap a(\Lambda_1) = \emptyset \\ M_C(s, \mu, \lambda)\,(1 - 2\overline{M}(\mu^*, \lambda^*)) & \text{otherwise} \end{cases} \quad (17)$$

where $\lambda^* \in \Lambda_1$ is a vertex point on the circle and in the plane $\Pi(s, \mu, \lambda)$, and μ^* is the angle of the line of intersection of $\Pi(s, \mu, \lambda)$ with the λ^*-detector. The function $M_C(s, \mu, \lambda)$ is defined as in equation (13) with the smooth solution of [5].

For the redundancy scheme of equations (16) and (17) to work, it is vital that the planes which intersect the circle nearly tangentially also intersect the complementary subpath $a(\Lambda_2)$. Therefore, for this method, the complementary part of the general circle-plus vertex path must intersect not only the planes which do not intersect the circle, but also the planes which are tangent and nearly tangent to the circle, more specifically the planes such that $|\cos\mu^*| < \sin\mu_0$. Since the value of μ_0 can be small, this *modified completeness condition* is only slightly more restrictive than Tuy's condition.

In summary, the filtered projections in the new composite algorithms are obtained:

- using the 2D stationary filter, equation (9), with M given by equation (16) for the circle data, $\lambda \in \Lambda_1$
- using equations (3) and (4) with the M function of equation (17) for $\lambda \in \Lambda_2$

D. Reconstruction of truncated CB projections

We discuss here the case where Ω is an infinite cylinder of radius r, oriented along the z-axis. The projections are truncated along z, and we attempt to reconstruct a finite cylindrical region Ω_h for which there exists a μ_0 such that the modified completeness condition of the path is satisfied.

The detector geometry of the circle-plus path remains the same as in section 4.A, except that for $\lambda \in \Lambda_2$ we now require the detector to be parallel to the z-axis, with the v-axis oriented along 1_z. The detector covers a region $\mathcal{D}(\lambda) = \{(u, v) | \, |u| < u_{\max}, v_{\min} < v < v_{\max}\}$, where $v_{\min}$ and $v_{\max}$ may depend on λ. The value of $u_{\max}$ is considered large enough to avoid truncation in u-direction. We denote the unmeasured region of the data as:

$$T(\lambda) = \{(u, v) | \; g(u, v, \lambda) \neq 0 \text{ and } (u, v) \notin \mathcal{D}(\lambda)\} \quad (18)$$

Kudo and Saito [7] have demonstrated that the composite algorithm can be used to reconstruct Ω_h if the values of $v_{\min}$ and $v_{\max}$ are appropriately chosen. We show here that the same property holds for the new composite algorithm. This is due to the fact that the 2D kernel applied to the scaled projections has a wedge-shaped support covering a limited angular region around the u-axis. Specifically, for any $\lambda \in (\Lambda_1 \bigcup \Lambda_2)$ the calculation of $g_F(u_0, v_0, \lambda)$ involves only the values of $g_S(u, v, \lambda)$ within a horizontal wedge $W(u_0, v_0, \lambda)$ centered on (u_0, v_0) and bounded by two lines $\mathcal{L}(s_1, \mu_1)$ and $\mathcal{L}(s_2, \mu_2)$, which contain (u_0, v_0) (the pairs (s_1, μ_1) and (s_2, μ_2) depend on u_0, v_0 and λ). Therefore, the filtered projection can be calculated from truncated data within the region

$$E(\lambda) = \left\{(u_0, v_0) | \; W(u_0, v_0, \lambda) \bigcap T(\lambda) = \emptyset\right\} \quad (19)$$

As can be seen from equation (5), the image $f_R(x)$ can be reconstructed at any point x_0 such that for all $\lambda \in (\Lambda_1 \bigcup \Lambda_2)$ the CB projection of x_0 onto the λ-detector belongs to the region $E(\lambda)$. The region of interest Ω_h can be reconstructed if, for all λ, the projection of Ω_h onto the detector is contained within $E(\lambda)$.

Let us briefly sketch how the wedge $W(u_0, v_0, \lambda)$ is determined for a given path. Consider first a vertex point along the circle ($\lambda \in \Lambda_1$). The scaled projections are filtered using the stationary filter of equation (9) with $M(s, \mu, \lambda) = \overline{M}(\mu, \lambda)$ given by equation (16). As discussed in section 3.B, the corresponding 2D convolution kernel has a wedge-shaped support of aperture $2\mu_0$ about the u-axis, and therefore,

$$W(u_0, v_0, \lambda) = \{(u, v) | \; |v - v_0| \leq |u - u_0| \tan\mu_0\} \quad (20)$$

Consider next a vertex point on the complementary subpath ($\lambda \in \Lambda_2$). From equations (3), (4) and (17), the calculation of $g_F(u_0, v_0, \lambda)$ only involves the value of $g_S(u, v, \lambda)$ along lines $\mathcal{L}(s, \mu)$ passing through (u_0, v_0) in the detector plane and such that $M(s, \mu, \lambda) \neq 0$. Observe from equation (17) that $M(s, \mu, \lambda) = 0$ where $\overline{M}(\mu^*, \lambda^*) = 1/2$, which corresponds to a plane $\Pi(s, \mu, \lambda)$ which intersects the circle $a(\Lambda_1)$ at two well-separated points (i.e. not "nearly tangentially"). This condition allows $W(u_0, v_0, \lambda)$ to be determined for a given path and for a given value of μ_0.

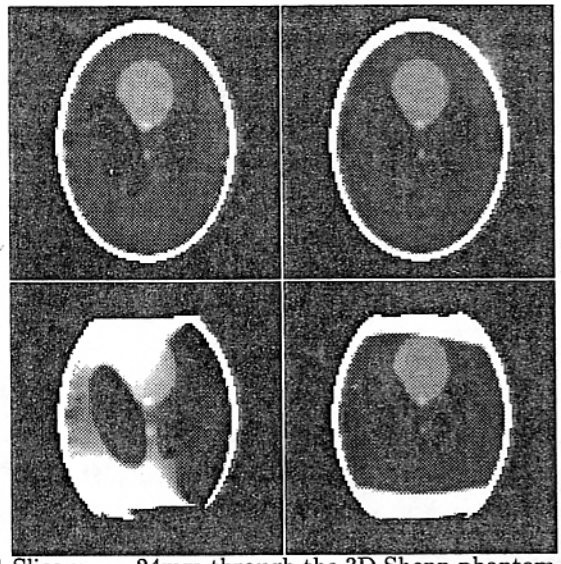

Fig. 1 Slice $y = -24$mm through the 3D Shepp phantom. Non-truncated data: (a) DC-FBP (b) New algorithm. Truncated data: (c) DC-FBP (d) New algorithm. The new composite algorithm is accurate and suited to handle truncated data

V. Implementation and simulations

Simulations were performed using the 3D Shepp phantom of intensity ranging from 1.0 to 2.0. The vertex path, located on a virtual cylinder of radius 300mm, consisted of a circle (120 vertex points) plus a one-turn helix (60 points). The pitch of the helix was chosen so that the path satisfies the modified completeness condition for $\mu_0 = \pi/15$. The vertex point was always a distance $D = 300$mm from the detector, and the CB angle for a circle point was $2 \times 18°$.

Non-truncated projections were collected considering a detector of 128×128 square pixels each of side 1.9mm. Truncation was introduced by reducing the number of pixels along the v-axis to 86. The data were reconstructed on a grid of 100^3 cubic voxels of side 2mm, using DC-FBP and the new composite algorithm. Images were displayed on a compressed greyscale ranging from 1.005 to 1.04.

Figures 1a,b show the slice $y = -24$mm for the case of non-truncated data. Despite careful implementation [8] of nonstationary filter, DC-FBP appears slightly more sensitive to discretization errors. The reconstruction cpu time on a SUN Ultra Sparcstation (167MHz) was 761s for DC-FBP and 403s for the new algorithm (See [9] for a detailed breakdown of reconstruction times). The new composite algorithm achieves faster and accurate reconstructions.

Figure 1c,d shows the same y-slice when data are axially truncated. DC-FBP yields reconstruction of poor quality. Artefacts are present throughout the image and the quantitative accuracy is poor. The new algorithm yields accurate reconstruction inside a certain region of interest, which demonstrates its ability to handle truncated data.

VI. Discussion and conclusions

A rigourous analysis of the CB reconstruction problem has been given for arbitrary circle-plus vertex paths. The composite algorithm of Kudo and Saito [9] has been shown to introduce singularities in some filtered projections even when the data are smooth. One way to handle this difficulty would be to ignore it and to rely on the discretization of the data to approximately integrate the singularities. We have derived a new exact composite algorithm which avoids the singularities and keeps the advantages, i.e. efficiency and ability to handle truncated data, of the original method of Kudo and Saito.

VII. Acknowledgement

F. Noo is a Research Assistant and M. Defrise is a Senior Researcher, both supported by the Belgian National Fund for Scientific Research. R. Clack and F. Noo were partially supported by a grant from the Whitaker Foundation, U.S.A.

VIII. References

[1] L. A. Feldkamp, L. C. Davis, J. W. Kress, "Practical cone-beam algorithm," J. Opt. Soc. Amer. A, A6, 612-619, 1984.

[2] H. Tuy, "An inversion formula for cone-beam reconstruction," SIAM J. Appl. Math., 43, 546-522, 1983.

[3] P. Grangeat, "Mathematical framework of cone-beam 3D reconstruction via the first derivative of the Radon transform," Mathematical methods in tomography, Herman, Louis and Natterer (eds.), Lecture Notes in Mathematics 1497, 66-97, Springer-Verlag, Berlin 1991.

[4] B. Smith, "Image reconstruction from cone-beam projections: Necessary and sufficient conditions and reconstruction methods," IEEE Trans. Med. Imag., 4, 14-28, 1985.

[5] M. Defrise and R. Clack, "A cone-beam reconstruction algorithm using shift variant filtering and cone-beam backprojection," IEEE Trans. on Med. Imag., 13, 186-195, 1994.

[6] H. Kudo, T. Saito, "Derivation and implementation of a cone-beam reconstruction algorithm for nonplanar orbits," IEEE Trans. Med. Imag., 13, 196-211, 1994.

[7] H. Kudo, T. Saito, "An extended completeness condition for exact cone-beam reconstruction and its application," IEEE Conf. Record 1994 Nuclear Science Symposium and Medical Imaging Conference, Norfolk, VA, 1710-14, 1995.

[8] C. Axelsson-Jacobson, M. Defrise, P. E. Danielsson, R. Clack, F. Noo, "Exact 3D-reconstruction using cone-beam backprojection, the Radon transform and linogram techniques," IEEE Conf. Record 1995 Nucl. Sci. Symp. and Med. Imag. Conf., San Francisco, CA, 1321-25, 1996.

[9] F. Noo, M. Defrise, R. Clack, T. J. Roney, T. A. White, S. G. Galbraith, "Stable and Efficient Shift-Variant Algorithm for Circle-plus-Lines Orbits in Cone-Beam C.T.", Proceedings ICIP-96: 1996 International Conference on Image Processing, Lausanne, September 1996, P. Delogne (ed). IEEE, Ceuterick, Leuven, Belgium, 539-542, 1996.